Dynamic Liquid-Liquid Interface: Applying Spinning Interfacial Microreactor to Actively Converge Biphasic Reactants for Enhanced Interfacial Reaction

Li Shiuan Ng,[1‡] Carice Chong,[1‡] Xin Yi Lok,[1‡] Veronica Pereira,[1] Zhi Zhong Ang,[1] Xuemei Han,[1] Haitao Li,[2] and Hiang Kwee Lee[1,3]*

[1] Division of Chemistry and Biological Chemistry, School of Physical and Mathematical Sciences, Nanyang Technological University, 21 Nanyang Link, Singapore 637371.

[2] School of Chemistry and Chemical Engineering, Yangzhou University, Yangzhou, 225002, PR China.

[3] Institute of Materials Research and Engineering, The Agency for Science, Technology and Research (A∗STAR), 2 Fusionopolis Way, #08-03, Innovis, 138634, Singapore.

‡ These authors contributed equally to this work.

*Correspondence to: hiangkwee@ntu.edu.sg

Keywords: biphasic reaction, dynamic microreactor, liquid-liquid interface, liquid marble, molecule transport

Abstract

Liquid-liquid interfacial reaction combines reactants with large polarity disparity to achieve greener and more efficient chemistry that is otherwise challenging in traditional single-phase systems. However, current interfacial approaches suffer from the need for a large amount of solvent/reactant/emulsifier and poor reaction performance arising from intrinsic thermodynamic constraints. Herein, we achieve efficient interfacial reaction by creating a magnetic-responsive, microscale liquid-liquid interface and exploit its dynamic spinning motion to generate vortex-like hydrodynamic flows that rapidly converge biphasic reactants to the point-of-reaction. Notably, the spinning of this functional interface at 800 rpm boosts reaction efficiency and its apparent equilibrium constant by >500-fold and 10^5-fold, respectively, higher than conventional methods that utilize bulk and/or non-dynamic liquid interface, even with external mechanical stirring. By driving reaction equilibrium towards favorable product formation, our unique design offers enormous opportunities to realize efficient multiphasic reactions crucial for diverse applications in chemical synthesis, environmental remediation, and even molecular recycling.

Introduction

Interfacial reaction at the boundary formed between two immiscible liquid phases is crucial to converge reactants with large polarity disparity (e.g., hydrophilic and hydrophobic molecules) for subsequent chemical transformations.[1-4] By enabling the reaction between solvent-incompatible reactants, liquid-liquid reaction potentially expedites the uncovering of novel chemistries to better exploit milder, greener, and more efficient reaction precursors/solvents that are otherwise difficult in traditional single-phase systems.[5-7] Current liquid-liquid reactions typically utilize a large volume of secondary liquid phase which, when combined with mechanical stirring and/or emulsifier, is necessary to boost interfacial contact area for cross-boundary molecular interactions/transfer.[8] Moreover, Pickering emulsion-based miniature reactors can also be employed to facilitate biphasic reaction by promoting mass transfers of both the hydrophilic and hydrophobic reactants.[9-12] For instance, biphasic heterogeneous solvent systems have enabled the catalytic reduction of p-nitroanisole with sodium borohydride, followed by the selective and spontaneous product extraction driven by the difference in solubility at the Pickering emulsion interface.[13] Despite its huge promise in various chemical, synthetic, and environmental applications, most interfacial designs are limited by the need for post-reaction removal of emulsifier additive and excess solvents to further purify/concentrate the product for downstream processes.[14, 15] It also remains a challenge to drive intrinsic interfacial reaction owing to the need for high reactants concentration to tackle the thermodynamic constraints (e.g., low equilibrium constant) imposed by constituting interfacial processes (e.g., adsorption, reaction, and/or desorption).[16]

Liquid marbles could address the aforementioned limitations by leveraging on their microliter-sized volume, excellent robustness in diverse liquid environments, and a unique

structural feature comprising of a microdroplet core encapsulated within a functional nanoparticle shell.[17, 18] These miniature platforms are highly versatile and can be easily incorporated with target properties (e.g. magnetic, photothermal, electric, plasmonic and self-propelling properties) through the huge library of nanomaterials and liquids available for microdroplet encapsulation.[19-22] In addition, liquid marbles can also be easily actuated with external forces (e.g., dielectrophoresis and electrostatic) or external mechanical rotation to manipulate the encapsulated microdroplet.[23-25] Notably, the formation of liquid marbles using magnetically active nanoparticles is an attractive approach to manoeuvre the encapsulated microdroplet on demand using a permanent magnet for diverse "lab in a droplet" applications.[26] Magnetic liquid marbles can also spin synchronously under a rotating magnetic field via the effective transduction of applied magnetic field to kinetic rotational energy by the magnetic coating. This process consequently drives a unique, centrifugal force-driven hydrodynamic phenomenon within the microdroplet for enhanced molecule transfer during chemical reactions.[27] While the dynamic actuation of liquid marbles provide opportunities for enhanced chemical reactions, the current use of liquid marbles as a miniature reactor is mainly restricted to single-phase processes in the embedded liquid microdroplet and/or gas-liquid interfacial reactions.[28-30] Moreover, the lack of study on the dynamic interactions between a spinning liquid marble and its exterior liquid environment also restricts its potential use for interfacial applications.

Herein, we achieve efficient interfacial reaction by utilizing magnetic-responsive liquid marble to create an active liquid-liquid interface formed between an encapsulated aqueous microdroplet and an exterior organic phase. This strategy exploits the magnetic particle shell as a magneto-to-mechanical transducer to effectively spin the miniature reactor, with the aim to induce vortex-like flows of reactants towards the target particle-assembled soft interface of miniature

reactor. Realizing such unique hydrodynamic flow is crucial to facilitate the convergence of immiscible reactants at the liquid boundary for enhanced biphasic reactions.

As a proof-of-concept demonstration, we use an environmentally relevant model reaction involving the interfacial deprotonation of organic-soluble bromothymol blue (a mutagenic and carcinogenic pollutant) into an aqueous-soluble product for effective decontamination.[31] Using the aqueous microdroplet as a reactant reservoir and product trap, the spinning of the interfacial reactor at 800 rpm achieves rapid reaction completion in ≤ 5 min and boosts reaction efficiency by ~530-fold relative to a non-dynamic bulk liquid interface. More importantly, our design evidently enhances the reaction's apparent equilibrium constant up to 3×10^5-fold better than conventional interfacial approaches, even under external mechanical stirring. Systematic investigations unveil that the active accumulation of reactants at a spinning liquid-liquid interface is the key to push the equilibrium constant towards product formation and drive interfacial reaction. By favouring product formation without needing excess reactants/solvents and/or heat energy inputs, our unique interfacial design offers valuable insights to realize efficient multiphasic reactions for chemical/material synthesis, environmental remediations, and waste valorization.

Results and Discussions

Dynamic manipulation of a liquid-liquid interface plays a central role in the rapid and active accumulation of reactants at the immiscible liquid boundary to facilitate their chemical transformation (Figure 1A). To create this functional liquid interface, we prepare the magnetic liquid marble by rolling an aqueous microdroplet of pre-defined volume (4 – 8 μL) on a bed of perfluorosilane-functionalized Fe_3O_4 nanoparticles (diameter, 13 ± 3 nm; Figure 1B; Figure S1).[19] Successful surface modification of the Fe_3O_4 nanoparticles is affirmed from their hydrophobicity (contact angle, 145°) and the emergence of the perfluorosilane's characteristic F 1s and Si 2p peaks in the XPS spectra (Figure 1C, Figure S2, S3).[32, 33] As-prepared liquid marble exhibits a three-dimensional sphere-like structure with the Fe_3O_4 nanoparticles localized at the air-water interface to form a robust, porous magnetic shell for effective microdroplet encapsulation (Figure 1D). Magnetic liquid marble can be easily manoeuvred in linear directions or actuated into a spinning motion in air simply by applying an external magnetic field (Figure S4). The liquid marble interacts stably with exterior liquid environments, whereby it floats on top of water or submerges into organic solvents (decane) because of their high or low surface tensions, respectively (Figure 1E). Both the excellent magnetic responsiveness and mechanical robustness of magnetic liquid marble inside an external liquid environment are important for its subsequent interfacial application.

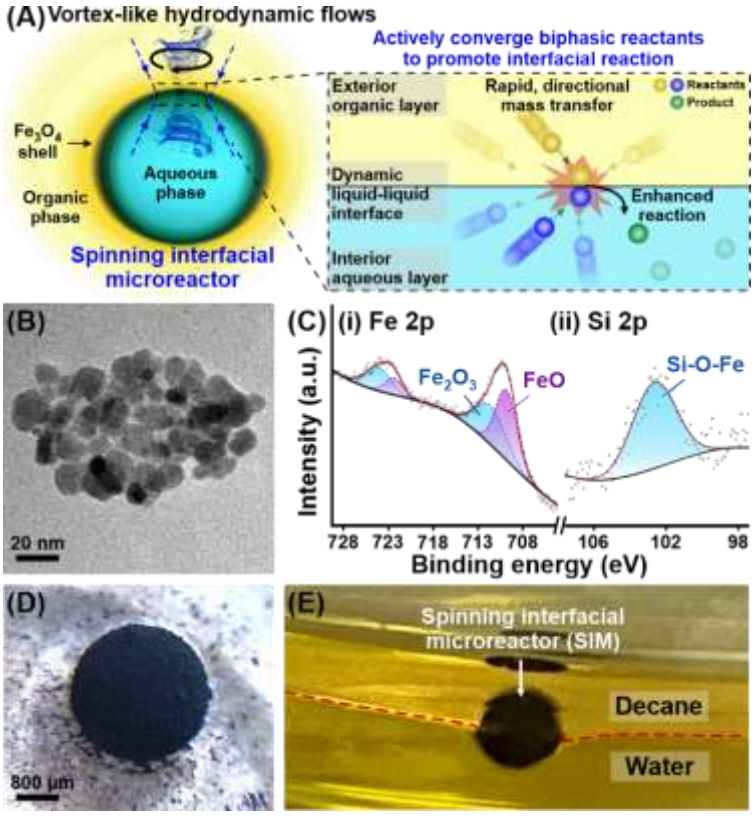

Figure 1. (A) Dynamic spinning of interfacial microreactor to actively accumulate reactants at immiscible liquid boundary for enhanced interfacial reaction. (B) TEM image of as-synthesized Fe_3O_4 nanoparticles. (C) High-resolution (i) Fe 2p and (ii) Si 2p XPS spectra affirm surface modification of Fe_3O_4 nanoparticles with perfluorosilane. (D) Digital image of a liquid marble coated with magnetic Fe_3O_4 nanoparticles. (E) Photograph of the interfacial microreactor floating on a decane-water interface.

To evaluate the potential use of magnetic liquid marble as an interfacial miniature reactor, we first characterize its spinning dynamics in an organic liquid medium when subjected to an applied rotating magnetic field (Figure 2A). Notably, the immersion of as-prepared liquid marble in an organic liquid phase allows the strategic positioning of Fe_3O_4 nanoparticles at the microscale oil-water boundary to achieve a magnetic-responsive soft interface. This design enables the

actuation of the ensemble on demand to create unique hydrodynamic flows for the active transportation of biphasic reactants towards the target interface. It is also noteworthy that an underlying bulk aqueous phase is used to reduce contact friction for the effective spinning of the miniature reactor under an applied rotating magnetic field (200-1200 rpm). A trace amount of white Al_2O_3 tracer is deposited atop of the liquid marble to allow accurate tracking using a high-speed optical camera for subsequent determination of the actual spin rate. For instance, we observe a magnetic liquid marble (6 μL) readily spins along its vertical axis when subjected to an applied rotating magnetic field (800 rpm) and requires ~75 ms to make one complete revolution (Figure 2B; Supplementary Video 1, 2). We also note no apparent loss of Fe_3O_4 nanoparticles from the interfacial microreactor when spinning, indicating that the magnetic building blocks are strongly adsorbed at the liquid-liquid interface. Collectively, these observations highlight that the liquid marble is spinning synchronously and stably with the applied magnetic field at 800 rpm, thereby exemplifying its ability for remote and rapid actuation even when submerged in a liquid medium.

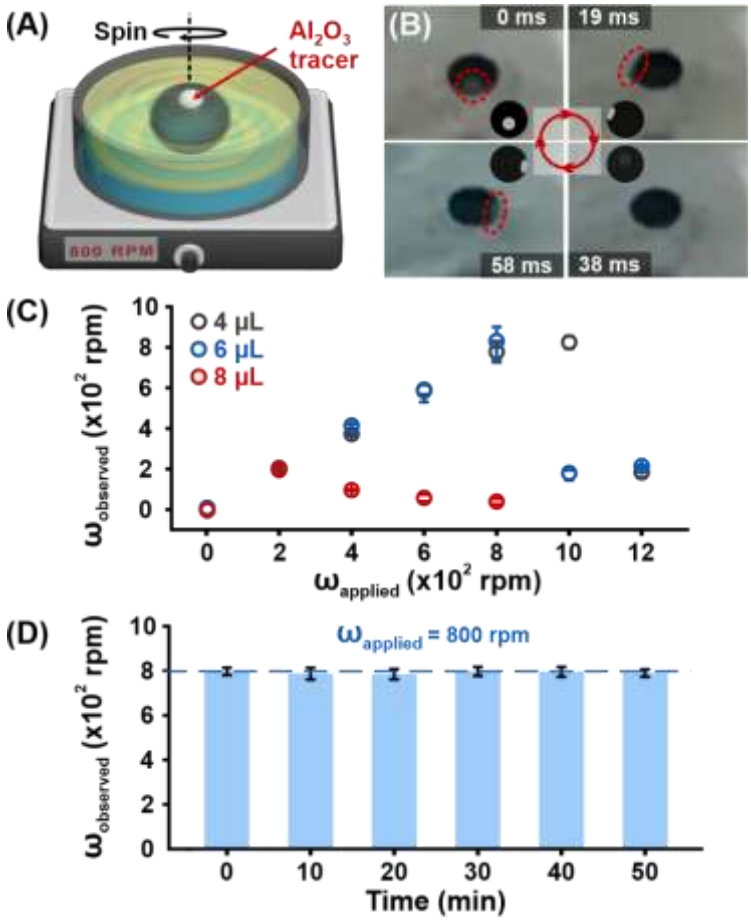

Figure 2. (A) Experimental set-up to investigate the interfacial microreactor's spinning dynamics in organic solvent. A rotating magnetic field is conveyed via a commercial stirrer. An underlying bulk aqueous phase is used to reduce contract friction and promote effective microreactor actuation. (B) Temporal snapshots of a spinning interfacial microreactor (6 µL) at 800 rpm. White Al_2O_3 powders are placed on its top to track its motion. (C) Observed spin rate of interfacial microreactor (volume, 4 - 8 µL) when subjected to an applied magnetic field rotating between 0 and 1200 rpm. (D) Interfacial microreactor spins synchronously and stably at 800 rpm for an extended duration of 50 min.

We also note the liquid marble's volumes (4 – 8 µL) have a direct impact on its spinning dynamics and its potential use as a dynamic interfacial miniature reactor (Figure 2C; Figure S5).

For liquid marbles with a volume ≤ 6 μL, they spin synchronously with the applied magnetic field as the rotational rate increases from 0 rpm to 800 rpm. Additional increases in the applied rotating magnetic field beyond 800 rpm leads to a plateau or even a decrease in the liquid marble's spin rates, possibly due to the higher inertia of the liquid marble and/or the drag resistance imposed by the fluid on the liquid marble when it is spinning at a faster rate.[34] We also observe that the use of a liquid marble with larger volume (8 μL) hinders efficient spinning, attaining a low maximum spin rate of 200 rpm despite the gradual increase in the applied rotating magnetic field to 800 rpm. This asynchronous motion is likely attributed to the smaller surface area-to-volume ratio when a larger microdroplet is used, whereby insufficient Fe_3O_4 nanoparticles are present at the liquid-liquid interface to effectively transduce the magnetic field into mechanical motion.[19] Nevertheless, the high tuneability and stability of the liquid marble's (with volume ≤ 6 μL) spinning dynamic over a prolonged duration of 50 min (< 2 % deviation in its spin rates) clearly highlight its suitability for interfacial application (Figure 2D). Our design is versatile and can be extended to other organic media (e.g. toluene and hexane; Figure S6) or different volumetric composition of bulk oil/aqueous phases (Figure S7) while maintaining its excellent magnetic responsiveness at 800 rpm. Hereon, we will term the 6 μL magnetic liquid marble as spinning interfacial microreactor (SIM) and use it for subsequent investigations because it possesses both the largest volumetric capacity and optimal maximum spin rate (e.g., 800 rpm) crucial for interfacial applications.

Having affirmed the effective spinning of the magnetic liquid marble in an external liquid, we subsequently employ this dynamic liquid-liquid interface to boost biphasic chemical reactions. The interfacial deprotonation of bromothymol blue (BTB) is chosen as a model reaction because of its relevance in environmental remediation whereby BTB is a pollutant with severe mutagenic

and carcinogenic effects (Figure 3A).[31] This organic pollutant exists in its protonated form (BTB, yellow appearance) when present in an organic medium or acidic solution (pH < 4) (Figure S8), whereas it deprotonates in an alkaline solution to form a negatively charged product (BTB^-, blue appearance).[35] The distinct color difference between the reactant and product consequently enables facile visual tracking of the interfacial reaction in real time. Using a control bulk interface formed between decane and aqueous (pH 9) phases, we observe slow interfacial deprotonation of BTB (0.08 mM; originally in decane) through the emergence of a faint blue layer (denoting product formation) only after a long duration of 30 min (Figure 3B). The sluggish reaction is likely due to the conventional use of a static liquid interface where slow, passive molecular diffusion dominates and is limited by intrinsic thermodynamic constraints.

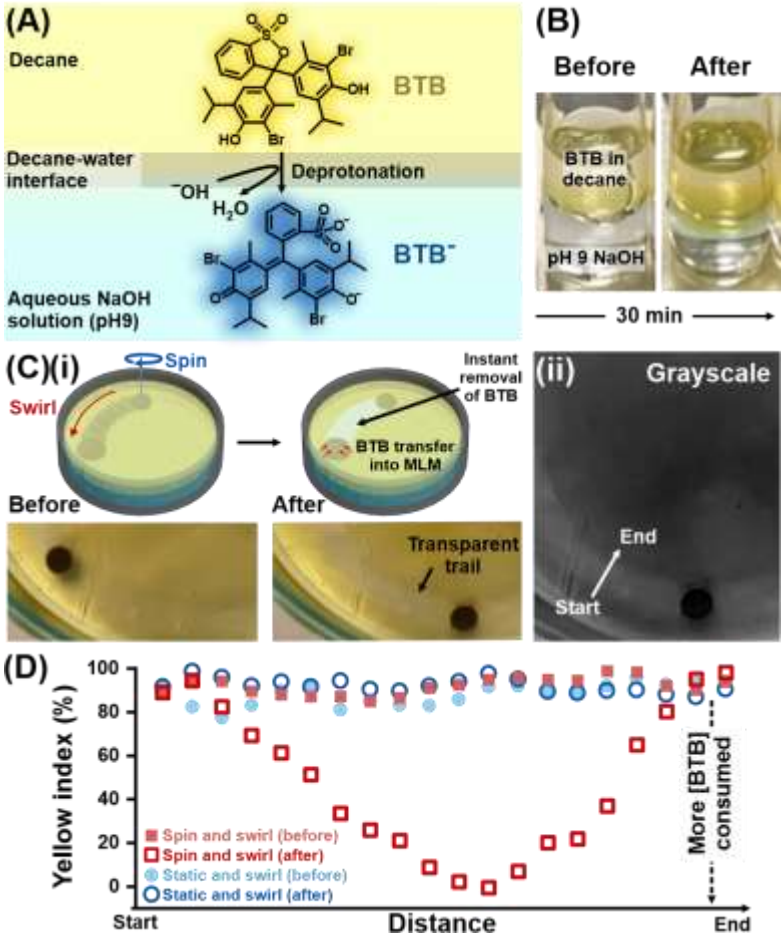

Figure 3. (A) Scheme illustrating the interfacial deprotonation of bromothymol blue (BTB) at decane-water boundary. (B) Digital images showing slow BTB deprotonation at the bulk interface formed between decane (contains BTB) and water (pH 9 NaOH solution) after 30 min. (C)(i) Scheme (top) and photographs (bottom) depicting the rapid decolorization of yellow BTB by a spinning interfacial microreactor and (ii) the associated grayscale image. (D) Quantitative image analysis to demonstrate the rapid decolorization of yellow reactant to leave a colorless trail behind the spinning interfacial microreactor.

To tackle this limitation, we form the spinning interfacial microreactor by encapsulating an alkaline microdroplet (6 μL, pH 9 NaOH solution) in a magnetic shell and immerse the ensemble into a decane solution containing BTB reactant (0.08 mM; Figure 3C). The aqueous core serves as (1) a reagent reservoir to deprotonate BTB and doubles as (2) a chemical trap to retain the anionic product for effective BTB decontamination in decane. We initiate the interfacial reaction by applying a rotating magnetic field at 800 rpm and concurrently swirl the miniature reactor in a circular path in decane for continuous decontamination. The reaction is tracked in situ by monitoring color changes in decane to avert potential complications arising from inaccurate extraction of the organic phase near the interfacial reactor and the diffusion of unreacted BTB from surrounding liquid regions. Notably, the spinning interfacial microreactor immediately decolorizes the yellow BTB solution to leave an obvious colorless trail as it moves around in the organic phase (Figure 3C; Supplementary Video 3). Quantitative image analysis on the temporal snapshots reveals ~95% reduction in the pixel values denoting yellowness in areas where the interfacial microreactor crosses, thereby indicating an obvious decrease in BTB concentration in these regions (Figure 3D). The decolorized regions in the organic solution spontaneously reverts to their original yellow appearance due to the replenishment of BTB reactants from the surrounding liquids (Figure

S9). We exclude potential loss of BTB reactants to the underlying bulk aqueous phase because the latter has an acidic pH that minimizes interfacial reaction and cross-boundary diffusion (Figure S8). In contrast, control experiments comprising of (1) a static liquid marble at identical pH 9 condition and (2) a spinning liquid marble containing an acidic solution (pH < 4) do not induce any apparent decolorization in decane, denoting negligible change to BTB concentration (Figure S10). The discoloration observed only in the case of a spinning interfacial microreactor affirms that an efficient interfacial reaction is indeed occurring at the dynamic liquid-liquid interface. This phenomenon is possibly driven by the vortex-like flows that originates from the spinning liquid interface, analogous to a rotating stir bar/object, which actively pull reactants from the bulk phases to the oil-water boundary for enhanced reaction (details to be discussed later).[36]

Similar to our observation in the exterior decane phase, we also note the rapid formation of blue BTB^- product in the encapsulated microdroplet by partially exposing the interfacial microreactor and *in situ* monitoring the color transitions (Figure 4A). It is worth mentioning that a semi-opened interfacial microreactor maintains its magnetic-responsiveness and spins effectively with a rotating magnetic field. Representative snapshots of the liquid marble notably unveil an initial colorless aqueous microdroplet gradually turning into an intense blue (Figure S11), as evident from the increase of pixel values denoting blueness from 3% to 96% at t = 0 s and t = 10 s, respectively (Figure 4A). The pixel value of the microdroplet remains relatively constant beyond 6 s, signifying that the interfacial reaction swiftly reaches an equilibrium in contrast to the faint blue appearance formed near a static bulk liquid interface after 30 min. We assure the observed color transitions are not caused by interference from the black Fe_3O_4 shell because subsequent expulsion of the aqueous microdroplet from the exposed microreactor (t = 16 s)

displays an obvious deep blue coloration (Figure S12). Interestingly, these findings highlight that the dynamic spinning of a neat liquid-liquid interface is the key factor to drive the interfacial reaction, even without the direct presence of Fe_3O_4 nanoparticles at the oil-water interface.

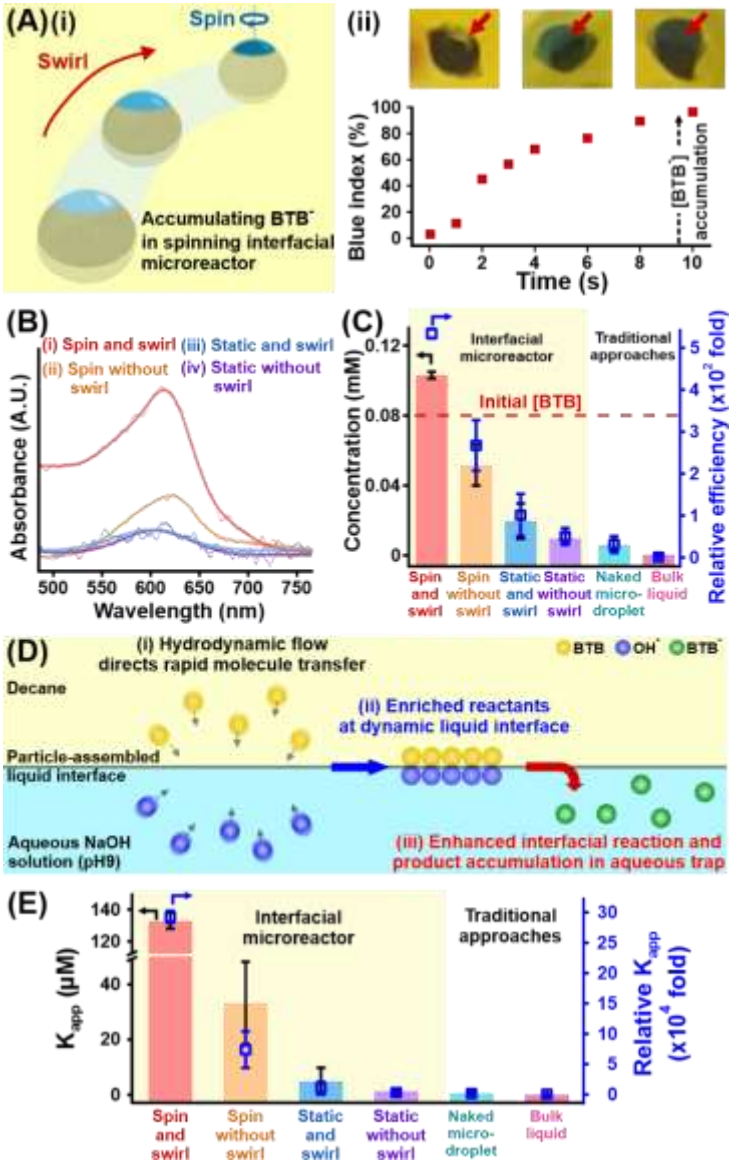

Figure 4. (A) Real-time visual monitoring of the formation and accumulation of blue BTB^- product in a partially opened spinning interfacial microreactor. (i) Scheme, (ii) digital images and quantitative image analysis of the temporal snapshots. (B) UV-vis absorption spectra comparing BTB^- product formation in the interfacial microreactor under four different experimental

conditions. (C) Comparison of BTB^- product concentration and relative decontamination/reaction efficiency of interfacial microreactor against conventional approaches utilizing bulk liquid interface and/or non-dynamic liquid-liquid interface. Reaction time and initial BTB reactant concentration are standardized at 5 min and 0.08 M, respectively. (D) Proposed mechanism on the use of dynamic, microscale liquid-liquid interface to boost interfacial reaction. (E) Comparison of the apparent reaction equilibrium constant (K_{app}) attained using our design and conventional interfacial approaches. For both (C) and (E), the relative efficiency and relative K_{app} are benchmarked against control experiment using bulk liquid interface.

To elucidate the origins of the enhanced interfacial reaction, we investigate the performances of a spinning interfacial microreactor under 4 different conditions, namely (i) spin and swirl, (ii) spin without swirl, (iii) static and swirl, and (iv) static without swirl at identical reaction conditions (Figure 4B). In a typical experiment, we extract the entire aqueous droplet at a predefined timing of 5 min and subsequently employ UV-vis absorption spectroscopy to quantify actual product concentration by comparing BTB^- characteristic peak at 616 nm with a standard calibration curve (Figure S13). Although our previous observation (Figure 4A) indicates that reaction equilibrium is likely attained within 10 s, we can only extract the embedded microdroplet at ~5 min due to the experimental challenges when attempting to perform this operation in < 5 min. Notably, our spinning interfacial microreactor under constant swirling in decane achieves the highest BTB^- formation of 0.103 mM in 5 min, even exceeding the initial BTB concentration (0.08 mM) by ~30 % (Figure 4C). We further justify that a reaction duration of 5 min is sufficient to reach reaction equilibrium, as demonstrated by the similar product concentration formed in the reactor (with < 7 % deviation) at t = 5 min and t = 25 min (Figure S14). Systematic comparisons across the four set-ups highlight the active spinning of the liquid-liquid interface as the main factor

to enhance interfacial reaction (~5-fold increment when comparing i and iii), whereas swirling contributes an additional ~2-fold improvement (comparing iii and iv) by directing the reactor to regions of higher reactant concentrations.

More importantly, our spinning interfacial microreactor achieves a ~530-fold and 10-fold higher yield of products than conventional interfacial designs that utilize (1) a bulk liquid interface or (2) a non-dynamic liquid-liquid interface built on a naked microdroplet, respectively, even when assisted with external mechanical stirring (Figure S15). By benchmarking against bulk interfacial reaction, the higher product formation in spinning interfacial microreactor translates to > 500-fold better decontamination/reaction efficiency even with a short reaction duration of 5 min (Figure 4C). From these experiments, we infer three important insights on the plausible mechanism behind the superior reaction performance of our unique interfacial design. First, microscale liquid-liquid interface facilitates interfacial reaction relative to a bulk interface due to its higher surface area-to-volume ratio. Second, the similar reaction efficiency between a static liquid marble and a naked microdroplet indicates that the Fe_3O_4 particle shell serves to actuate the liquid-liquid interface but does not aid in cross-boundary molecule transfer via intermediate adsorption on the particle surfaces. Third, the spinning of the actual microscale liquid-liquid interface is critical to enhance biphasic reaction, which otherwise cannot be achieved through external mechanical stirring by a commercial stir bar even at a similar speed of 800 rpm. Such dynamic manipulation of the particle-assembled soft interface is expected to drag neighbouring liquid layers into a circular motion and creates centrifugal forces in both the exterior organic phase and interior aqueous phase (Figure 4D). These centrifugal forces consequently induce vortex-like hydrodynamic flows originating from the dynamic liquid interface, actively converging reactants from both the organic and

aqueous phases onto the liquid-liquid boundary to promote collision probability and the consequential chemical interactions/reactions.[27, 36]

Interestingly, the enrichment of biphasic reactants directly at the point-of-reaction is beneficial to drive the forward process of the equilibrium reaction (in this case, BTB ⇌ BTB^- + H^+; Figure 4E), in accordance with the *Le Chatelier's* principle.[37] We verify a shift in the reaction equilibrium by quantifying the reactant and product concentrations at t = 5 min (i.e., time to reach equilibrium) to determine the apparent equilibrium constant (K_{app}), whereby a higher K_{app} denotes higher product formation. Notably, spinning interfacial microreactor achieves the highest K_{app} of 1.33×10^{-4} M, which is ~110-fold and 3×10^5-fold better than a static liquid marble and a conventional reaction set-up involving bulk liquid interface, respectively (Supporting Information 1). We thus demonstrate the unprecedented use of a dynamic, microscale liquid interface to manipulate reaction equilibrium towards efficient interfacial reaction, even under the same reaction conditions and with ~10^3-fold lesser solvent volume used. This unique advantage offered by our interfacial design enables better utilization of both the reaction solvents and reactants by tackling the intrinsic thermodynamic bottleneck that cannot be achieved simply by increasing the reaction volume.[8, 16] Moreover, the Fe_3O_4 particle coating can be easily removed from the reaction using a permanent magnet, which is straightforward compared to the extensive post-reaction treatments required to remove emulsifier additives in conventional methods.[19, 27]

Conclusion

In conclusion, we have achieved efficient interfacial reaction by dynamically manipulating a microscale liquid-liquid interface formed using a magnetic-responsive liquid marble. Our strategy effectively utilizes the spinning motion of an interfacial microreactor to induce vortex-like hydrodynamic flows originating from the nanoparticle-assembled soft interface, thereby actively converging biphasic reactants towards the interfacial boundary for rapid reactions. By using an environmental decontamination reaction as a model, our dynamic platform spinning at 800 rpm swiftly reaches a reaction equilibrium in ≤5 min and achieves a >500-fold superior decontamination efficiency compared to a static counterpart. More importantly, our design drastically boosts the apparent thermodynamic equilibrium constant by up to 10^5-fold when compared to traditional approaches comprising of bulk liquid interface and/or non-dynamic microscale liquid-liquid interface, even under external mechanical stirring.

Our approach is versatile and presents an attractive chemical handle to effectively manipulate interfacial reaction towards favorable product formation, with the aim to tackle the intrinsic thermodynamic constraints of interfacial processes. Achieving this ensemble of benefits is crucial to enable greener chemical transformation by minimizing the need for additional heat energy input and/or high reactant concentrations that are often employed in traditional chemistry to promote product formation. Together with its simple fabrication, high manoeuvrability and ease of post-reaction removal, our unique design of a dynamic liquid-liquid interface offers valuable insights to boost multiphasic reactions that are beneficial for diverse (bio)chemical, energy, and environmental applications.

Experimental

Chemicals. Iron (II) chloride, iron (III) chloride, 1H,1H,2H,2H-perfluorooctyltriethoxysiliane (≥ 97 %), Al_2O_3 (CG-20), ammonium hydroxide solution (28–30 %, ACS reagent), sodium hydroxide (≥ 98 %), 1-butanol (≥ 99.4 %, ACS reagent) and bromothymol blue (dye content, ≥ 95 %) were purchased from Sigma-Aldrich. Ethanol (≥ 99.8 %, absolute), decane (≥ 95 %), hexane (HPLC grade), and toluene (HPLC grade) were purchased from Thermo Fisher Scientific. All chemicals were used without further purification. Milli-Q water (> 18.0 MΩ.cm) was purified with a Sartorius Arium 611 ® UV ultrapure water system.

Synthesis of Fe_3O_4 nanoparticles. The fabrication of Fe_3O_4 nanoparticles was carried out using the protocol described in literature. Briefly, aqueous NH_4OH solution (1.5 M) was added dropwise to 200 mL water/ethanol (4:1 v/v) containing $FeCl_3$ (3.14 mmol), $FeCl_2$ (1.51mmol), and 1H,1H,2H,2H-perfluorooctyltriethoxysiliane (0.20 mL) under nitrogen protection and vigorous stirring until pH 8. After overnight stirring, the precipitate was isolated from the solution with a bar magnet, washed with copious amount of water and ethanol by high-speed centrifugation. This step was repeated thrice, and the precipitate was dried in oven at 65 ^oC for 2 – 3 hours. The Fe_3O_4 nanoparticles were subsequently pulverized to obtain fine powders and stored under nitrogen condition for further use.

Fabrication of spinning interfacial microreactor. Magnetic liquid marbles were formed by rolling 4 – 8 μL aqueous droplets on a bed of pulverized perfluorooctyltriethoxysiliane–functionalized Fe_3O_4 nanoparticles.

Evaluation of interfacial microreactor's spinning dynamics under applied rotating magnetic field. For spinning evaluation, 4 – 8 μL liquid marble was first fabricated and transferred to a bulk liquid-liquid interface (top liquid phase, 2 mm decane; bottom liquid phase, 5 mm water) in a petri

dish that was placed on top of a commercial magnetic stirrer plate. Trace amount of Al_2O_3 was deposited on top of the interfacial microreactor to track its orientation, while the underlying aqueous layer served to reduce contact friction as the microreactor spins. The rotating field was then activated and pre-set at 200 – 1200 rpm. The entire set-up was allowed to equilibrate for 10 s and the spinning dynamics were subsequently captured using a high-speed optical camera (240 fps). All experiments were repeated thrice to ensure the reproducibility of the results.

Evaluation of the effect of liquid height on interfacial microreactor's spinning dynamics. The effect of liquid height of both the underlying aqueous phase and bulk decane phase was performed using a 6 μL spinning interfacial microreactor. Decane and water heights were varied from 1-3 mm and 5-7 mm, respectively. The experiments were repeated thrice and recorded using a high-speed optical camera (240 fps).

Quantitative image analyses to determine reactant consumption and product formation. The optical images were processed and split into respective red, green and blue channels using ImageJ. To quantitatively compare the concentration of yellow BTB reactant present, the grayscale image formed using the blue channel was selected to analyse the yellow index of the image because of its highest sensitivity towards a yellow-to-colorless transition. In general, a more intense yellow coloration denotes higher BTB concentration. The yellow index was calculated using the following equation.

$$Yellow\ index\ (\%) = (1 - \frac{normalized\ pixel\ value}{maximum - minimum\ pixel\ value}) \times 100\%$$

where each set of data is subtracted with the minimum pixel value to normalize the baseline pixel value.

Similarly, the concentration of blue BTB^- product concentration can be quantitatively compared by using a grayscale image formed from the red channel because of its highest sensitivity

towards a blue-to-colorless transition. In general, a more intense blue coloration denotes higher BTB^- concentration. The blue index was calculated using the following equation.

$$Blue\ index\ (\%) = (1 - \frac{normalized\ pixel\ value}{maximum - minimum\ pixel\ value}) \times 100\%$$

where each set of data is subtracted with the minimum pixel value to normalize the baseline pixel value.

Quantification of deprotonated bromothymol blue (BTB^-). A calibration curve relating absorption intensity with BTB^- concentration was first established for subsequent product quantification in the reaction solution. Bromothymol blue (BTB) was first dissolved in aqueous NaOH solution and further serial-diluted to various concentration between 10^{-6} M and 10^{-5} M. The adsorption spectra were obtained using UV-vis absorption spectroscopy and further used for quantification using the characteristic peak at 616 nm.

Application of spinning interfacial microreactor for environmental remediation application. The model reaction chosen involved the interfacial deprotonation reaction of bromothymol blue (BTB) as an organic dye pollutant. In a typical experiment, 6 μL aqueous NaOH solution (pH 9) was encapsulated within the spinning interfacial microreactor and subsequently transferred to a decane solution (with < 1 % of 1-butanol) containing dissolved BTB (0.08 mM) which layered over an acidic aqueous layer (pH < 4). The interfacial microreactor was spun and concurrently swirled in the decane phase for 5 min. After which, the embedded reaction droplet was extracted and the BTB^- product concentration was quantified using UV-vis absorption spectroscopy. All experimental were repeated at least thrice to ensure the reproducibility of the results. The same reaction was also conducted for 25 mins.

Interfacial deprotonation of BTB using traditional approaches. For bulk liquid interface, equal volume of decane solution (with < 1 % of 1-butanol) containing BTB reactant (0.08 mM) was

added onto an aqueous NaOH (pH 9) layer. After external mechanical stirring using a commercial stir bar at 800 rpm for 5 mins, the aqueous NaOH layer was extracted for UV-vis absorption spectroscopy measurement.

For a non-dynamic microscale liquid-liquid interface, a 6 μL aqueous NaOH (pH 9) microdroplet was added into a decane solution (with < 1 % of 1-butanol) containing BTB reactant (0.08 mM). After external mechanical stirring using a commercial stir bar at 800 rpm for 5 mins, the microdroplet was extracted and BTB^- product concentration was measured using UV-vis absorption spectroscopy. The same experiment was also conducted but in the absence of any mechanical stirring.

All experimental were repeated at least thrice to ensure the reproducibility of the results.

Characterization. Transmission electron microscopy (TEM) images were collected on a JEM-1400 (JEOL) operated at 100 kV. Contact angles were measured on a Theta Lite tensiometer equipped with a Firewire digital camera. Static contact angles were measured with a 5 μL ultrapure water droplet. XPS spectra were measured using a Phoibos 100 spectrometer with a monochromatic Mg X-ray radiation source. Optical camera was used to capture the slow-motion video (240 fps) of spinning liquid marble. UV-vis spectroscopic measurements were conducted using an AvaSpec-ULS2048CL-EVO-UA-50 equipped with a deuterium-halogen light source (AvaLight-DH-S).

ASSOCIATED CONTENT

Supporting Information

The following files are available free of charge.

Experimental details, synthesis of Fe_3O_4 nanoparticles, fabrication of spinning interfacial microreactor, evaluation of interfacial microreactor's spinning dynamics under applied rotating magnetic field, evaluation of the effect of liquid height on interfacial microreactor's spinning dynamics, quantitative image analyses to determine reactant consumption and product formation, quantification of deprotonated bromothymol blue (BTB^-), application of spinning interfacial microreactor for environmental remediation application, interfacial deprotonation of BTB using traditional approaches and characterization (PDF). Supplementary Videos highlighting the spinning of interfacial miniature reactors and their application in interfacial reaction are also included.

AUTHOR INFORMATION

Corresponding Author

*E-mail hiangkwee@ntu.edu.sg (H.K.L.).

Author Contributions

The manuscript was written through contributions of all authors. All authors have given approval to the final version of the manuscript. ‡These authors contributed equally.

ACKNOWLEDGMENT

L.S.N., C.C. and X.Y.L. contributed equally to this work. H.K.L. thanks the funding supports from Singapore Ministry of Education (AcRF Tier 1 RS13/20 and RG4/21), A*STAR Singapore (AME YIRG A2084c0158), and Nanyang Technological University start-up grants. The research was conducted as a part of NICES (NTU-IMRE Chemistry Lab for Eco Sustainability; REQ0275931), a joint research initiative between Nanyang Technological University (NTU) and Institute of Materials Research and Engineering (IMRE) from Agency for Science, Technology and Research (A*STAR).

REFERENCES

1. Piradashvili, K.; Alexandrino, E. M.; Wurm, F. R.; Landfester, K., Reactions and Polymerizations at the Liquid–Liquid Interface. *Chem. Rev.* **2016,** *116* (4), 2141-2169.
2. Xue, F.; Zhang, Y.; Zhang, F.; Ren, X.; Yang, H., Tuning the Interfacial Activity of Mesoporous Silicas for Biphasic Interface Catalysis Reactions. *ACS Appl. Mater. Interfaces* **2017,** *9* (9), 8403-8412.
3. Wei, Y.; Cheng, G.; Ho, H.-P.; Ho, Y.-P.; Yong, K.-T., Thermodynamic Perspectives on Liquid–Liquid Droplet Reactors for Biochemical Applications. *Chem. Soc. Rev.* **2020,** *49* (18), 6555-6567.
4. Cortés, E.; Besteiro, L. V.; Alabastri, A.; Baldi, A.; Tagliabue, G.; Demetriadou, A.; Narang, P., Challenges in Plasmonic Catalysis. *ACS Nano* **2020,** *14* (12), 16202-16219.
5. Fan, H.; Wang, J.; Wu, P.; Zheng, L.; Xiang, J.; Liu, H.; Han, B.; Jiang, L., Hydrophobic Ionic Liquid Tuning Hydrophobic Carbon to Superamphiphilicity for Reducing Diffusion Resistance in Liquid-Liquid Catalysis Systems. *Chem* **2021,** *7* (7), 1852-1869.
6. Zhang, Y.; Ettelaie, R.; Binks, B. P.; Yang, H., Highly Selective Catalysis at the Liquid–Liquid Interface Microregion. *ACS Catal.* **2021,** *11* (3), 1485-1494.
7. Pera-Titus, M.; Leclercq, L.; Clacens, J.-M.; De Campo, F.; Nardello-Rataj, V., Pickering Interfacial Catalysis for Biphasic Systems: From Emulsion Design to Green Reactions. *Angew. Chem. Int. Ed.* **2015,** *54* (7), 2006-2021.
8. Khoo, K. S.; Leong, H. Y.; Chew, K. W.; Lim, J.-W.; Ling, T. C.; Show, P. L.; Yen, H.-W., Liquid Biphasic System: A Recent Bioseparation Technology. *Processes* **2020,** *8* (2).
9. Yan, S.; Zou, H.; Chen, S.; Xue, N.; Yang, H., Janus Mesoporous Silica Nanosheets with Perpendicular Mesochannels: Affording Highly Accessible Reaction Interfaces for Enhanced Biphasic Catalysis. *Chem. Commun.* **2018,** *54* (74), 10455-10458.

10. Hao, Y.; Hao, S.; Li, Q.; Liu, X.; Zou, H.; Yang, H., Metal-Nanoparticles-Loaded Ultrathin g-C3N4 Nanosheets at Liquid–Liquid Interfaces for Enhanced Biphasic Catalysis. *ACS Appl. Mater. Interfaces* **2021,** *13* (39), 47236-47243.
11. Li, C.; Liu, S.; Pi, Y.; Feng, J.; Liu, Z.; Li, S.; Tan, R., Ionic Liquid-Functionalized Amphiphilic Janus Nanosheets Afford Highly Accessible Interface for Asymmetric Catalysis in Water. *J. Catal.* **2021,** *395*, 236-245.
12. Ni, L.; Yu, C.; Wei, Q.; Liu, D.; Qiu, J., Pickering Emulsion Catalysis: Interfacial Chemistry, Catalyst Design, Challenges, and Perspectives. *Angew. Chem. Int. Ed.* **2022,** *61* (30), e202115885.
13. Tan, H.; Zhang, P.; Wang, L.; Yang, D.; Zhou, K., Multifunctional amphiphilic carbonaceous microcapsules catalyze water/oil biphasic reactions. *Chem. Commun.* **2011,** *47* (43), 11903-11905.
14. Santos, J. H. P. M.; Carretero, G.; Coutinho, J. A. P.; Rangel-Yagui, C. O.; Ventura, S. P. M., Multistep Purification of Cytochrome c PEGylated Forms Using Polymer-Based Aqueous Biphasic Systems. *Green Chem.* **2017,** *19* (24), 5800-5808.
15. Mack, K.; Doeker, M.; Grabowski, L.; Jupke, A.; Rother, D., Extractive In Situ Product Removal For The Application of Naturally Produced L-Alanine as an Amine Donor in Enzymatic Metaraminol Production. *Green Chem.* **2021,** *23* (13), 4892-4901.
16. Vaida, V., Prebiotic Phosphorylation Enabled by Microdroplets. *Proc. Natl. Acad. Sci. U.S.A.* **2017,** *114* (47), 12359-12361.
17. Saczek, J.; Yao, X.; Zivkovic, V.; Mamlouk, M.; Wang, D.; Pramana, S. S.; Wang, S., Long-Lived Liquid Marbles for Green Applications. *Adv. Funct. Mater.* **2021,** *31* (35), 2011198.
18. Xue, Y.; Wang, H.; Zhao, Y.; Dai, L.; Feng, L.; Wang, X.; Lin, T., Magnetic Liquid Marbles: A "Precise" Miniature Reactor. *Adv. Mater.* **2010,** *22* (43), 4814-4818.
19. Han, X.; Lee, H. K.; Lim, W. C.; Lee, Y. H.; Phan-Quang, G. C.; Phang, I. Y.; Ling, X. Y., Spinning Liquid Marble and Its Dual Applications as Microcentrifuge and Miniature Localized Viscometer. *ACS Appl. Mater. Interfaces* **2016,** *8* (36), 23941-23946.
20. Han, X.; Koh, C. S. L.; Lee, H. K.; Chew, W. S.; Ling, X. Y., Microchemical Plant in a Liquid Droplet: Plasmonic Liquid Marble for Sequential Reactions and Attomole Detection of Toxin at Microliter Scale. *ACS Appl. Mater. Interfaces* **2017,** *9* (45), 39635-39640.
21. Gao, W.; Lee, H. K.; Hobley, J.; Liu, T.; Phang, I. Y.; Ling, X. Y., Graphene Liquid Marbles as Photothermal Miniature Reactors for Reaction Kinetics Modulation. *Angew. Chem. Int. Ed.* **2015,** *54* (13), 3993-3996.
22. Ooi, C. H.; van Nguyen, A.; Evans, G. M.; Gendelman, O.; Bormashenko, E.; Nguyen, N.-T., A Floating Self-Propelling Liquid Marble Containing Aqueous Ethanol Solutions. *RSC Adv.* **2015,** *5* (122), 101006-101012.
23. Ooi, C. H.; Jin, J.; Sreejith, K. R.; Nguyen, A. V.; Evans, G. M.; Nguyen, N.-T., Manipulation of a Floating Liquid Marble using Dielectrophoresis. *Lab Chip* **2018,** *18* (24), 3770-3779.

24. Nguyen, N.-K.; Singha, P.; An, H.; Phan, H.-P.; Nguyen, N.-T.; Ooi, C. H., Electrostatically Excited Liquid Marble as a Micromixer. *Reaction Chemistry & Engineering* **2021,** *6* (8), 1386-1394.
25. Nguyen, N.-K.; Singha, P.; Dai, Y.; Rajan Sreejith, K.; Tran, D. T.; Phan, H.-P.; Nguyen, N.-T.; Ooi, C. H., Controllable High-Performance Liquid Marble Micromixer. *Lab Chip* **2022,** *22* (8), 1508-1518.
26. Zhao, Y.; Xu, Z.; Niu, H.; Wang, X.; Lin, T., Magnetic Liquid Marbles: Toward "Lab in a Droplet". *Adv. Funct. Mater.* **2015,** *25* (3), 437-444.
27. Han, X.; Lee, H. K.; Lee, Y. H.; Ling, X. Y., Dynamic Rotating Liquid Marble for Directional and Enhanced Mass Transportation in Three-Dimensional Microliter Droplets. *J. Phys. Chem. Lett.* **2017,** *8* (1), 243-249.
28. Han, X.; Lee, H. K.; Lee, Y. H.; Hao, W.; Liu, Y.; Phang, I. Y.; Li, S.; Ling, X. Y., Identifying Enclosed Chemical Reaction and Dynamics at the Molecular Level Using Shell-Isolated Miniaturized Plasmonic Liquid Marble. *J. Phys. Chem. Lett.* **2016,** *7* (8), 1501-1506.
29. Huang, J.; Cheng, F.; Binks, B. P.; Yang, H., pH-Responsive Gas–Water–Solid Interface for Multiphase Catalysis. *J. Am. Chem. Soc.* **2015,** *137* (47), 15015-15025.
30. Rong, X.; Ettelaie, R.; Lishchuk, S. V.; Cheng, H.; Zhao, N.; Xiao, F.; Cheng, F.; Yang, H., Liquid Marble-Derived Solid-Liquid Hybrid Superparticles for CO2 Capture. *Nat. Commun.* **2019,** *10* (1), 1854.
31. Zhou, Y.; Lu, J.; Zhou, Y.; Liu, Y., Recent Advances for Dyes Removal Using Novel Adsorbents: A Review. *Environ. Pollut.* **2019,** *252*, 352-365.
32. Yin, Y.; Ren, Y.; Lu, J.; Zhang, W.; Shan, C.; Hua, M.; Lv, L.; Pan, B., The nature and catalytic reactivity of UiO-66 supported Fe3O4 nanoparticles provide new insights into Fe-Zr dual active centers in Fenton-like reactions. *Appl. Catal., B* **2021,** *286*, 119943.
33. Huang, L.; Lu, C.; Wang, F.; Dong, X., Piezoelectric Property of PVDF/Graphene Composite Films Using 1H, 1H, 2H, 2H-Perfluorooctyltriethoxysilane as a Modifying Agent. *J. Alloys Compd.* **2016,** *688*, 885-892.
34. Khaw, M. K.; Ooi, C. H.; Mohd-Yasin, F.; Nguyen, A. V.; Evans, G. M.; Nguyen, N.-T., Dynamic Behaviour of a Magnetically Actuated Floating Liquid Marble. *Microfluid Nanofluidics* **2017,** *21* (6), 110.
35. Shalaby, A. A.; Mohamed, A. A., Determination of Acid Dissociation Constants of Alizarin Red S, Methyl Orange, Bromothymol Blue and Bromophenol Blue Using a Digital Camera. *RSC Adv.* **2020,** *10* (19), 11311-11316.
36. Mohamed-Ibrahim, N. A. b.; Kheng Boong, S.; Zhong Ang, Z.; Shiuan Ng, L.; Tan, J. Y. C.; Chong, C.; Kwee Lee, H., Applying Magnetic-Responsive Nanocatalyst-Liquid Interface for Active Molecule Manipulation to Boost Catalysis Beyond Diffusion Limit. *ChemCatChem* **2022,** *14* (10), e202200036.
37. Klotz, E.; Doyle, R.; Gross, E.; Mattson, B., The Equilibrium Constant for Bromothymol Blue: A General Chemistry Laboratory Experiment Using Spectroscopy. *J. Chem. Educ.* **2011,** *88* (5), 637-639.

Table of Contents